ISSN 1027-5495. Functional Materials, 28, No.1 (2021), p. 42-48.
doi:https://doi.org/10.15407/fm28.01.42 © 2021 — STC "Institute for Single Crystals"

Nanostructured $CuFe_2O_4$ and $CuFe_2O_4$/reduced graphene oxide composites: structural and magnetic studies

***V.O.Kotsyubynsky*[1], *R.I.Zapukhlyak*[1], *V.M.Boychuk*[1], *M.A.Hodlevska*[1], *I.P.Yaremiy*[1], *Kh.V.Bandura*[2], *A.I.Kachmar*[1], *S.V.Fedorchenko*[1], *M.A.Hodlevskyi*[1]**

[1]V. Stefanyk Precarpathian National University, 57 Shevchenko St., 76018 Ivano-Frankivsk, Ukraine
[2]Ivano-Frankivsk National Medical University, 2 Halytska St., 76018 Ivano-Frankivsk, Ukraine

Received Juny 10, 2020

In this work the effect of annealing in the range of 200–500°C on the phase composition, morphological properties and magnetic microstructure of hydrothermally synthesized $CuFe_2O_4$ and $CuFe_2O_4$/reduced graphene oxide has been investigated using XRD, SEM, Mossbauer spectroscopy and low temperature nitrogen adsorption methods. The influence of the presence of reduced graphene oxide particles on the parameters of hyperfine interaction for the composite material has been observed. The evolution of pore size distribution for the synthesized samples with increasing of annealing temperature has been traced.

Keywords: reduced graphene oxide, copper ferrite, Mossbauer spectroscopy, pore size distribution.

Нанорозмірні $CuFe_2O_4$ та композит $CuFe_2O_4$/відновлений оксид графену: дослідження структури та магнітних властивостей. *В.О.Коцюбинський, Р.І.Запухляк, В.М.Бойчук, М.А.Годлевська, І.П.Яремій, Х.В.Бандура, А.І.Качмар, С.В.Федорченко, М.А.Годлевський*

Досліджено вплив відпалу у температурному діапазоні 200–500°C на фазовий склад, морфологічні властивості та магнітну мікроструктуру гідротермально синтезованих $CuFe_2O_4$ та композиту $CuFe_2O_4$/відновлений оксид графену з використанням методів рентгеноструктурного аналізу, скануючої електронної мікроскопії, месбауерівської спектроскопії та низькотемпературної адсорбції азоту. Спостерігався вплив присутності частинок відновленого оксиду графену у композитному матеріалі на параметри надтонкої взаємодії зразка. Простежено еволюцію розподілу пор за розмірами синтезованих зразків із ростом температури відпалу.

Исследовано влияние отжига в температурном диапазоне 200–500°C на фазовый состав, морфологические свойства и магнитную микроструктуру гидротермально синтезированных $CuFe_2O_4$ и композита $CuFe_2O_4$/восстановленный оксид графена с использованием методов рентгеноструктурного анализа, сканирующей электронной микроскопии, мессбауэровской спектроскопии и низкотемпературной адсорбции азота. Наблюдалось влияние присутствия частиц восстановленного оксида графена в композитном материале на параметры сверхтонкого взаимодействия образца. Прослежена эволюция распределения пор по размерам синтезированных образцов с ростом температуры отжига.

1. Introduction

Copper spinel $CuFe_2O_4$ has various practical applications as a catalyst in water-gas shift synthesis [1] and oxidative destruction of hazardous pollutants [2], as a biologically active agent [3] and a material for gas sensors [4]. $CuFe_2O_4$ is a *p*-type semiconductor with a band gap of about 1.3–1.5 eV that is suitable for photocatalytic applications in the visible range for photo-Fenton [5] and hydrogen evolution [6] reactions. This material was successfully tested as an anode for Li-ion power cells [7]. The performance of $CuFe_2O_4$ ferrite as a functional material can be improved by combining it with graphene and reduced graphene oxide (rGO). The $CuFe_2O_4$/rGO composite demonstrates a high catalytic activity under visible light irradiation [8], in particular, phenol hydroxylation [9]. These materials are tested as high sensitive and selective sensors of NH_3 at room temperature [10]. The $CuFe_2O_4$/graphene composites demonstrate enhanced performance as electrodes for supercapacitors (specific capacitance of about 640 F/g with excellent charge/discharge cycling stability [11]). Due to their high magnetic characteristics, nanostructured spinel ferrites are widely investigated [12] and copper spinel $CuFe_2O_4$ is not an exception. In this work, a study of magnetic and structural properties of nanosized $CuFe_2O_4$ ferrite and $CuFe_2O_4$/rGO composite materials obtained by hydrothermal route has been carried out.

2. Experimental

$CuFe_2O_4$ nanoparticles were obtained by the hydrothermal route using $Fe_2(SO_4)_3{\cdot}6H_2O$, $CuSO_4{\cdot}5H_2O$ and NaOH. The graphene oxide colloidal solution was obtained by the Hummers method [13] and used during the $CuFe_2O_4$/rGO synthesis with the same experimental protocol details. The predicted mass ratio of oxide and graphene components is 2:1. The samples were annealed at temperatures of 300–500°C in an argon atmosphere.

The structural properties of the materials were investigated by the XRD method (Cu–K_α radiation with a Ni–K_β-filter). The structural models for cubic and tetrahedral $CuFe_2O_4$ were based on the ICSD#37429 and #16666, respectively [14]. Average sizes and shapes of coherently scattering domains (CSD) were determined by the analysis of broadening diffraction reflections using the Scherrer equation. A combination of Gaussian and Cauchy functions was used to approximate the XRD profiles. The presence of microstrains was neglected.

^{57}Co Mossbauer spectra (a MS-1104Em spectrometer) were obtained under thermally stabilized conditions (temperature accuracy is ±1 K). The isomeric shift was calibrated relative to the α–Fe standard (line width of 0.29 mm/s). The model fitting was performed using the Mosswin 3.0 software. The specific surface area (S_{BET}, m^2/g, determined using the multipoint BET method) and pore size distribution (PSD, obtained using the DFT approach [15]) were measured by the method of nitrogen adsorption at 77.2 K (a Quantachrome NOVA 2200e porosimeter) with previous degassing at 180°C for 10–12 h.

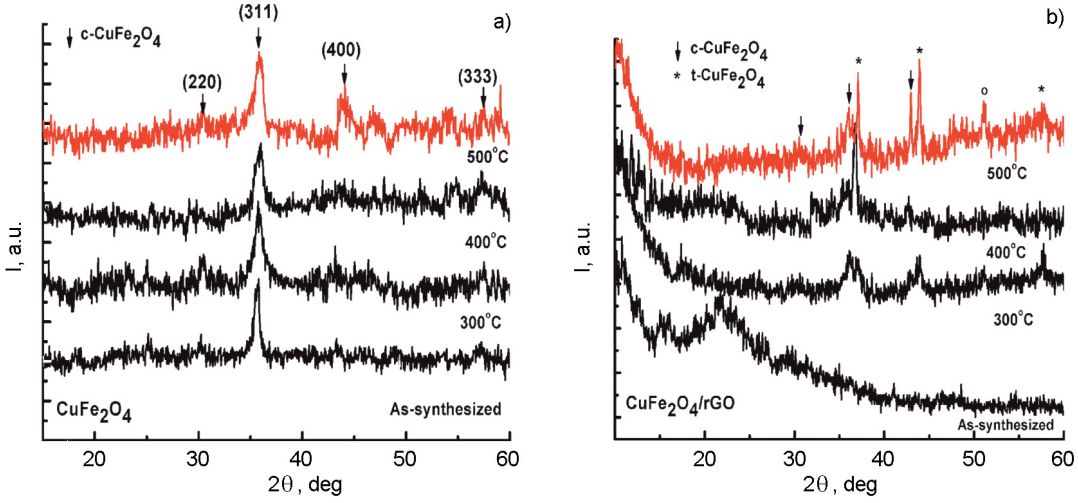

Fig. 1. XRD patterns of hydrothermally synthesized (a) $CuFe_2O_4$ and (b) $CuFe_2O_4$/rGO composite materials annealed at different temperatures.

3. Results and discussion

The structure of $CuFe_2O_4$ is formed by a close-packed lattice of oxygen ions with basic cubic symmetry. Besides, the presence of Cu^{2+} ions in an orbital degenerate state causes the collective distortion effect (Jahn-Teller effect) with symmetry changing from cubic to tetrahedral one [16]. The symmetry changes are observed typically for $CuFe_2O_4$ synthesized at temperatures higher than 900–1000°C with the following slow cooling [17].

The broadened peak in the XRD pattern of the as-synthesized powder corresponds to cubic $CuFe_2O_4$ spinel (Fig. 1a). Only the reflections of a cubic spinel phase (c–$CuFe_2O_4$) were observed. Annealing in argon atmosphere causes an increase in FWHM of main (311) reflection, which indicates a decrease in the average particle size at a temperature of 100–300°C with subsequent stabilization and growth after annealing at 500°C. The average particle sizes of ferrite powders annealed at a temperature of 300–500°C are in the range of 7–9 nm with a tendency to growing, which corresponds to a slight decrease in the S_{BET} values. The correlation between structural and morphological parameters for as-synthesized $CuFe_2O_4$ (Fig. 2) indicates a relatively low agglomeration degree.

As-synthesized $CuFe_2O_4$/rGO is amorphous but annealing at 300°C causes a two-phase material formation: characteristic reflections of tetrahedral (t–$CuFe_2O_4$) and cubic (c–$CuFe_2O_4$) structures are observed.

The direct calculation of an average particle size is difficult, but annealing leads to fast enlarging of the copper ferrite average particle size, moreover, the rate of growth of t–$CuFe_2O_4$ particles is relatively high. An increase in the annealing temperature up to 500°C leads to an increase in the average particle size but the crystallinity of the materials remains low.

The evolution of PSD in the synthesized samples as a result of an increase in the annealing temperature was traced using the methods of low-temperature nitrogen adsorption (Fig. 3) and DFT [18].

As-synthesized $CuFe_2O_4$ is characterized by a mesoporous structure with pore sizes of 3–20 nm and the most probable pore size of about 5 nm (Fig. 3a). The surface morphology of as-synthesized $CuFe_2O_4$/rGO is much developed but the micropores content is very low (Fig. 3a). The PSD curve is non-smooth and has several maxima indicating the presence of several fractions of particles

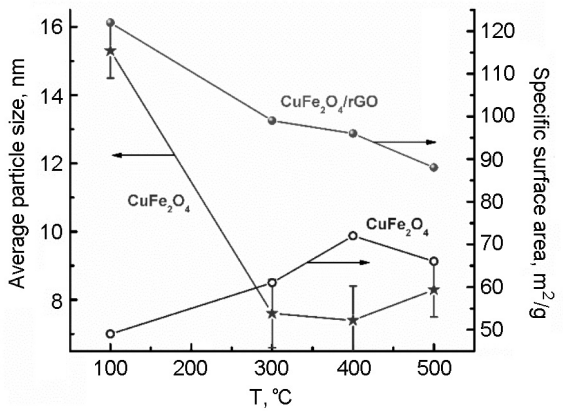

Fig. 2. CSD size and specific surface area of cubic $CuFe_2O_4$ as a function of annealing temperature.

with different sizes. The position of the main maximum at about 6 nm does not depend on the temperature increase. An increase in the annealing temperature up to 400°C for $CuFe_2O_4$ causes an increase in the content of small-size pores. Besides, annealing leads to an increase in the density of $CuFe_2O_4$/rGO without a significant change in the pore size.

The Mossbauer spectroscopy allows obtaining additional information about the structure of the materials. Cu^{2+} and Fe^{3+} ions are in crystalline and magnetic non-equivalent tetrahedral and octahedral sites, respectively. The $CuFe_2O_4$ is a partially inverse spinel, so the cation distribution can be described as $(Cu_xFe_{1-x})_A[Cu_{1-x}Fe_{1+x}]_BO_4$, where x is the inversion parameter ($x = 0$ and $x = 1$ denote inverse and normal spinel, respectively). SEM images of as-synthesized $CuFe_2O_4$ and $CuFe_2O_4$/rGO are presented in Fig. 4.

Room temperature (290 K) Mossbauer spectra of the as-synthesized $CuFe_2O_4$ consist of both doublet and sextet components (Fig. 5a). The annealing leads to a step-by-step decrease in the total intensity of the doublet components up to 11 % for $CuFe_2O_4$ annealed at 500°C. Fitting procedures made it possible to determine the parameters of hyperfine interactions: isomeric shift I_s, quadrupole splitting Q_s, hyperfine magnetic field induction H_{hf} (for sextets), linewidth G, integral intensity S (Table 1). In all the cases, the doublet components are due to the presence of spinel particles with sizes that allow the transition to a single-domain state with a shorter relaxation time of the magnetic moments compared to the data measurement time (excited state lifetime of ^{57}Fe nucleus is 141.8 ns) [19].

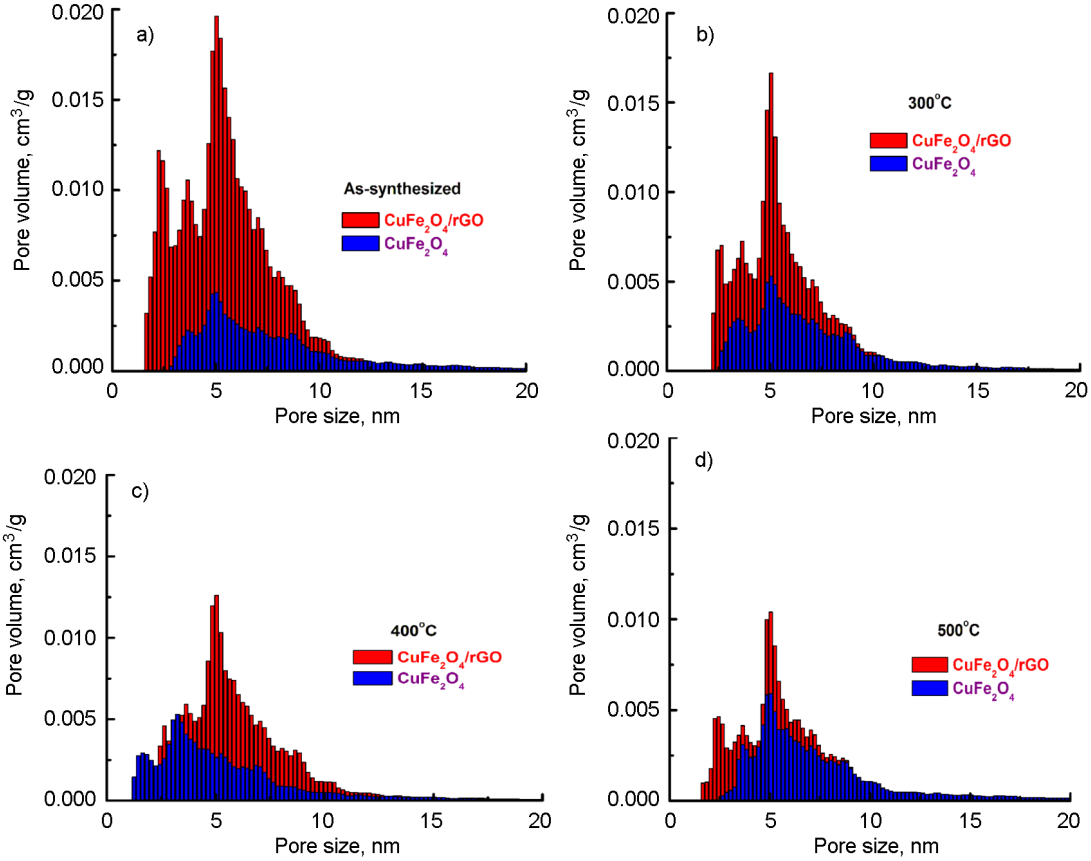

Fig. 3. Adsorption/desorption isotherms and pore size distribution for as-synthesized (a) and annealed at 300–500°C (b–d) $CuFe_2O_4$ and $CuFe_2O_4$/rGO samples.

Magnetically ordered parts of the spectra were fitted as a superposition of two sextet components corresponding to the presence of ^{57}Fe ions in tetrahedral and octahedral sites of the spinel structure. In general, the ratio between integral intensities of these components equals to the number of Fe^{3+} ions in A- and B-sites of spinel (inversion degree). In addition, in the case of ultrasmall particles, the contribution of "surface" and "bulk" Fe^{3+} ions with different close environments is important, since an increase in the surface-to-volume ratio for nanoparticles leads to an increase in the signals from ^{57}Fe located in the A-sites of the spinel structure [20]. Mossbauer measurements were carried out at 90 K for verification of the origin of superparamagnetic components (Fig. 5c, d). The spectra obtained for as-synthesized $CuFe_2O_4$ consist of two ordered magnetic sextets (Fig. 5, c).

The Neel time of magnetic moment relaxation is calculated as $\tau_N = \tau_0 \exp(KV/kT)$, where τ_0 is the characteristic time of the material (for spinel materials it usually falls into the interval of 10^{-9} s to 10^{-11} s), K is the magnetocrystalline anisotropy constant, V is the nanoparticle volume, T is the temperature. The magnetocrystalline anisotropy constant for $CuFe_2O_4$ is $0.6 \cdot 10^4$ J/m^3 [21], so, for $\tau_0 = 10^{-10}$ s, the critical particle size is about 8 nm. The identification of the $CuFe_2O_4$ sublattice at 90 K was based on the relatively higher H_{hf} values for ^{57}Fe nuclei in octahedral sites (B-sublattice) [22]. The ratio between the subspectrum fractional areas corresponding to A- and B- sublattices is 0.94. The ratio of the recoilless absorption probabilities for ^{57}Fe nuclei in tetra- and octahedral surroundings is about 0.94 [23], so, the inverse degree is close to 1 and the estimated cation distribution for pure $CuFe_2O_4$ sample is $(Fe)_A[CuFe]_BO_4$. The SA/S_B ratio for as-synthesized $CuFe_2O_4$ at room temperature is about 0.93; therefore, the probabilities of the transition from the magnetically ordered to the superparamagnetic state for Fe^{3+} ions in A- and B-sites are very close. Annealing at 300°C causes a decrease in the S_A/S_B ratio to 0.61 that corresponds to the inversion degree of about 0.84. An increase in the annealing temperature to 400 and 500°C leads to the formation of a spinel structure with an inversion degree of 0.86 and 0.76, respectively.

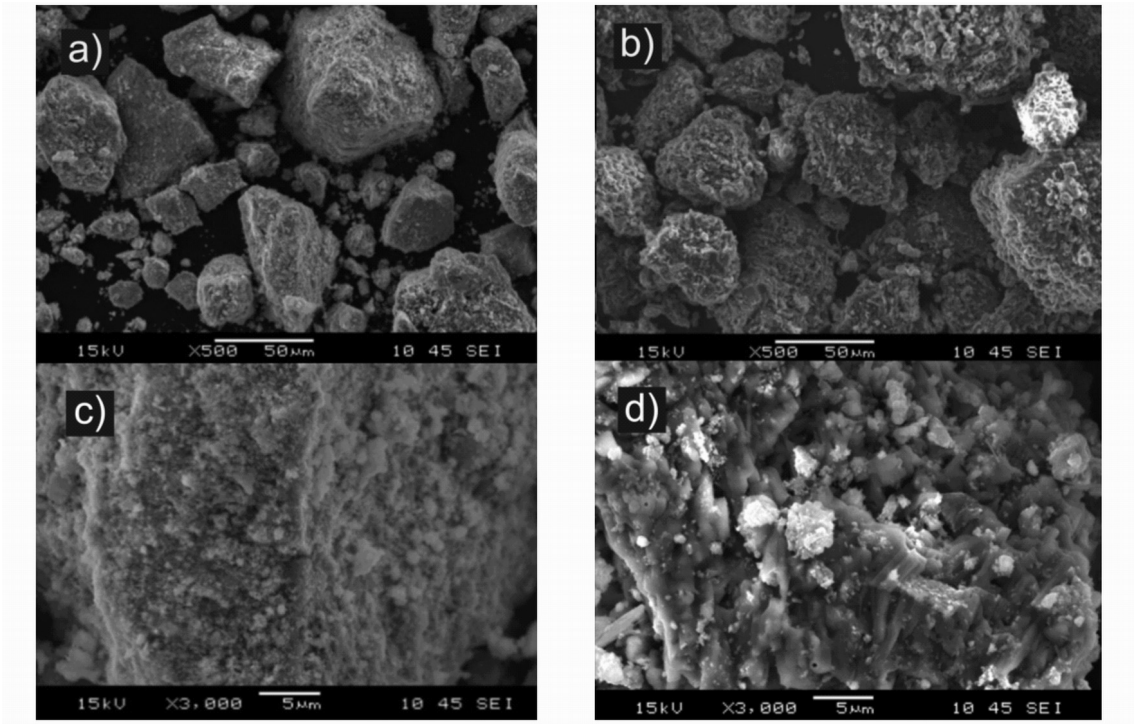

Fig. 4. SEM images of as-synthesized (a) $CuFe_2O_4$ and (b) $CuFe_2O_4$/rGO.

Table 1. Mossbauer parameters for $CuFe_2O_4$

Site	I_s, mm/s	Q_s, mm/s	H_{hf}, T	S, %	G, mm/s
As-synthesized					
B	0.29	0.01	45.7	30.2	0.71
A	0.29	−0.05	41.3	32.7	1.12
D1	0.36	0.58		22.3	0.43
D2	0.24	0.01		14.8	1.55
As-synthesized (90 K)					
A	0.3631	−0.02	49.4	48.77	0.70
B	0.4833	0.00	51.3	50.57	0.99
300 °C					
B	0.30	−0.01	45.7	40.9	0.63
A	0.30	−0.03	41.4	25.3	1.21
D1	0.34	0.68		21.5	0.51
D2	0.28	0.05		12.3	2.28
400 °C					
B	0.30	−0.07	47.2	50.5	0.76
A	0.28	0.02	42.9	33.4	1.43
D	0.31	0.72		16.0	0.6
500 °C					
B	0.29	−0.02	471.3	58.5	0.75
A	0.27	−0.06	426.8	30.2	1.2
D	0.33	0.73		11.3	0.54

The $CuFe_2O_4$/rGO materials, both as-synthesized and treated at 300°C, are paramagnetic (Fig. 5b). At the same time, Mossbauer spectra for as-synthesized $CuFe_2O_4$/rGO at 90 K (Fig. 5d) are formed by a combination of very broadened doublet and sextet components corresponding to an intermediate stage between magnetically ordered and superparamagnetic states of the particles. As a result, the average particle size of as-synthesized $CuFe_2O_4$/rGO does not exceed 8–10 nm and remains in the superparamagnetic state at 90 K.

Annealing at 400°C causes the appearance of a weak magnetic ordering. For $CuFe_2O_4$/rGO annealed at 500°C, the sextet components coexist with a central broadened doublet (Fig. 5b). This sample consists of *c*- and *t*–$CuFe_2O_4$ modifications, but its separation is impossible. The Mossbauer spectrum of this material measured at 295 K was optimally separated into two magnetic sextets with hyperfine fields of about 48.3 T and 44.6 T corresponding to octahedral and tetrahedral sites, respectively (Table 2).

These values are relatively lowered compared to results presented in [24]; this can be explained by the effect of the presence of rGO fragments in the pores of ferrite particles, which disturb the superexchange interaction and lead to hyperfine field decreasing.

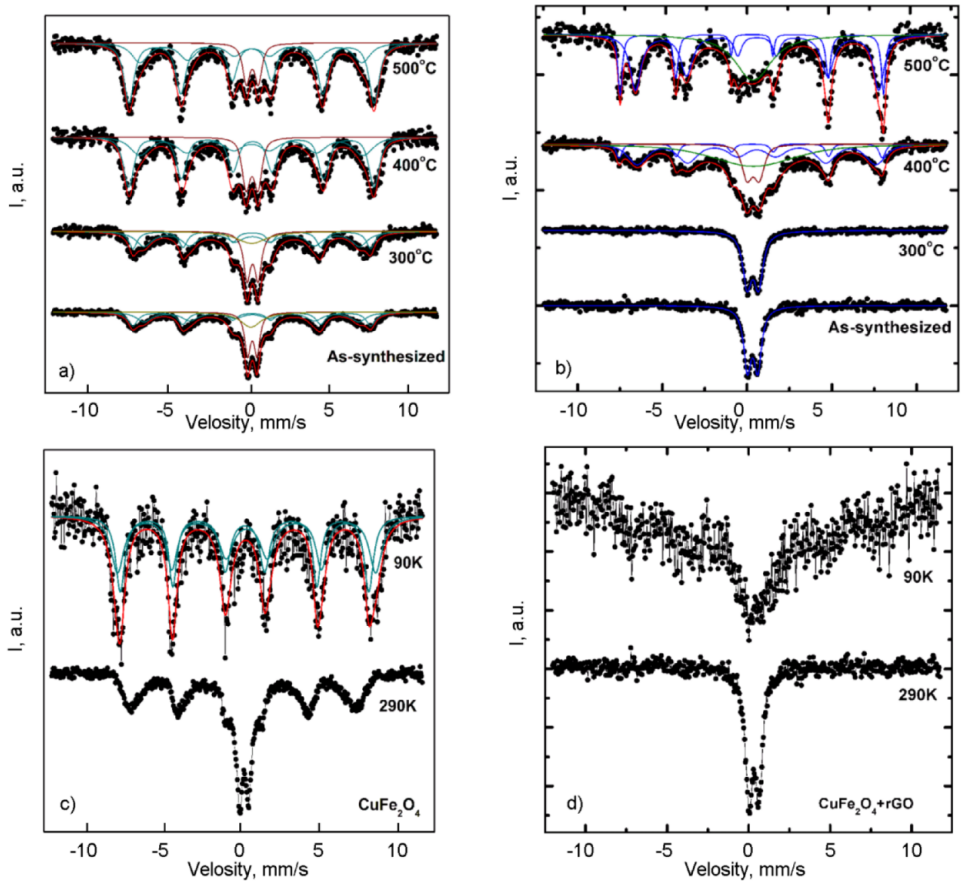

Fig. 5. Mossbauer spectra of (a) $CuFe_2O_4$ and (b) $CuFe_2O_4$/rGO annealed at different temperatures (all the spectra are measured at 290 K) and Mossbauer spectra of (c) as-synthesized $CuFe_2O_4$ and (d) $CuFe_2O_4$/rGO measured at 290 K and 90 K.

Table 2. Mossbauer parameters for $CuFe_2O_4$/rGO

$CuFe_2O_4$/rGO					
Site	I_s, mm/s	Q_s, mm/s	H_{hf}, T	S,. %	G, mm/s
As-synthesized					
D	0.33	0.61	–	100	0.54
300 °C					
D	0.34	0.68	–	100	0.63
400 °C					
B	0.27	–0.09	48.3	8.0	0.37
A	0.57	0.04	43.9	38.3	1.18
D	0.36	0.63		13.1	0.70
Sg	0.35			40.6	5.06
500 °C					
B	0.28	–0.01	48.3	20.7	0.30
A	0.59	0.01	44.6	48.9	0.77
D	0.36	0.67		30.4	2.27

4. Conclusions

Ultrafine $CuFe_2O_4$ and $CuFe_2O_4$/rGO were prepared by the hydrothermal method. The effect of annealing in the range of 200–500°C on the phase state, morphology and magnetic properties was investigated. The obtained materials were characterized by XRD, Mossbauer spectroscopy, low temperature nitrogen adsorption and SEM. The experimental results showed that upon annealing, the synthesized $CuFe_2O_4$/rGO composites crystallize in both the tetrahedral (t–$CuFe_2O_4$) and cubic (c–$CuFe_2O_4$) phases of copper ferrite, while the materials obtained without rGO at different temperatures are ultrafine c–$CuFe_2O_4$. The inversion degree of hydrothermally obtained $CuFe_2O_4$ decreases from 1 for the as-synthesized sample to 0.76 for the sample annealed in argon atmosphere at 300°C. With an increase in the annealing temperature, a gradual decrease in the specific surface area of the $CuFe_2O_4$/rGO composite material and a simultaneous decrease in the values of

hyperfine fields for both octahedral and tetrahedral positions of Fe^{3+} localization was interpreted as a result of the presence of rGO particles in the pores of ferrite particles.

Acknowledgment. This work was supported by the National Research Foundation of Ukraine (Project 2020.02/0043).

References

1. M.Estrella, L.Barrio, G.Zhou et al., *J.Phys. Chem.C*, **113**, 14411 (2009).
2. R.Wu, J.Qu, H.He, Y.Yu, *Appl.Catal.B*, **48**, 492004 (2004).
3. S.Kanagesan, M.Hashim, S.AB Aziz et al., *Appl.Sci.*, **6**, 184 (2016).
4. M.A.Haija, A.F.Abu-Hani, N.Hamdan et al., *J.Alloys Compd.*, **690**, 4619 (2017).
5. J.Gao, S.Wu, Y.Han et al., *J.Colloid Interface Sci*, **524**, 409 (2018).
6. H.Yang, J.Yan, Z.Lu et al., *J.Alloys Compd.*, **476**, 715 (2009).
7. Z.Xing, Z.Ju, J.Yang et al., *Electrochim. Acta*, **102**, 51 (2013).
8. P.Chen, X.Xing, H.Xie et al., *Chem.Phys. Lett.*, **660**, 176 (2016).
9. Y.Zhao, G.He, W.Dai, H.Chen, *Ind.Eng. Chem.Res.*, **53**, 12566 (2014).
10. L.S.K.Achary, A.Kumar, B.Barik et al., *Sens. Actuators B*, **272**, 100 (2018).
11. R.Khan, M.Habib, M.A.Gondal et al., *Mater. Res.Express*, **4**, 105501 (2017).
12. L.Kaykan, A.K.Sijo, A.Zywczak et al., *Appl. Nanosci. (in print) (2020).*
13. V.M.Boychuk, V.O.Kotsyubynsky, K.V.Bandura et al., *J.Nanosci.Nanotechnol.*, **19**, 7320 (2019).
14. E.Prince, R.G.Treuting, *Acta Crystallogr.*, **9**, 1025 (1956).
15. J.Landers, G.Y.Gor, A.V.Neimark, *Colloids Surf.,A*, **437**, 3 (2013).
16. I.Nedkov, R.E.Vandenberghe, T.Marinova et al., *Appl.Surf.Sci.*, **253**, 2589 (2006).
17. B.J.Evans, S.S.Hafner, *J.Phys.Chem.Solids*, **29**, 1573 (1968).
18. J.P.Olivier, W.Conklin, M.V.Szombathely, *Stud.Surf.Sci.Catal.*, **87**, 81 (1994).
19. V.Kotsyubynsky, V.Moklyak, A.Hrubiak, *Mater.Sci.-Pol.*, **32**, 481 (2014).
20. G.F.Goya, H.R.Rechenberg, *Nanostruct. Mater.*, **10**, 1001 (1998).
21. I.Nedkov, R.E.Vanderberghe, G.Vissokov et al., *Phys.Status Solid, A*, **201**, 1001 (2004).
22. R.K.Selvan, C.O. Augustin, V.Sepelak et al., *Mater.Chem.Phys.*, **112**, 373 (2008).
23. S.Da Dalt, A.S.Takimi, T.M.Volkmer et al., *Powder Technol.*, **210**, 103 (2011).
24. J.Z.Jiang, G.F.Goya, H.R.Rechenberg, *J. Phys.: Condens.Matter,* **11**, 4063 (1999).